1− and 2+ discrete states in Zr90 populated via the (O17,O'17γ) reaction

F.C.L. Crespi, A. Bracco, R. Nicolini, E.G. Lanza, A. Vitturi, D. Mengoni, S. Leoni, G. Benzoni, N. Blasi, C. Boiano S. Bottoni, et al.

1^- and 2^+ discrete states in ^{90}Zr populated via the (^{17}O,^{17}O$'\gamma$) reaction

F. C. L. Crespi,[1,2] A. Bracco,[1,2,*] R. Nicolini,[1,2] E. G. Lanza,[3] A. Vitturi,[4,5] D. Mengoni,[4,5] S. Leoni,[1,2] G. Benzoni,[2] N. Blasi,[2] C. Boiano,[2] S. Bottoni,[1,2] S. Brambilla,[2] F. Camera,[1,2] A. Corsi,[1,2,†] A. Giaz,[2] B. Million,[2] L. Pellegri,[1,2] V. Vandone,[1,2] O. Wieland,[2] P. Bednarczyk,[6] M. Ciemała,[6,‡] M. Kmiecik,[6] M. Krzysiek,[6] A. Maj,[6] D. Bazzacco,[5] M. Bellato,[5] B. Birkenbach,[7] D. Bortolato,[4,5] E. Calore,[8] B. Cederwall,[9] G. de Angelis,[8] P. Désesquelles,[10] J. Eberth,[7] E. Farnea,[5] A. Gadea,[11] A. Görgen,[12] A. Gottardo,[4,8] H. Hess,[7] R. Isocrate,[5] J. Jolie,[7] A. Jungclaus,[13] R. S. Kempley,[14] M. Labiche,[15] R. Menegazzo,[5] C. Michelagnoli,[4,5,§] P. Molini,[8] D. R. Napoli,[8] A. Pullia,[1,2] B. Quintana,[16] F. Recchia,[4,5] P. Reiter,[7] E. Sahin,[8,‖] S. Siem,[12] P.-A. Söderström,[17,¶] O. Stezowski,[18] Ch. Theisen,[19] C. Ur,[5] and J. J. Valiente-Dobón[8]

[1]*Dipartimento di Fisica dell'Università degli Studi di Milano, I-20133 Milano, Italy*
[2]*INFN, Sezione di Milano, I-20133 Milano, Italy*
[3]*INFN, Sezione di Catania, I-95123 Catania, Italy*
[4]*Dipartimento di Fisica dell'Università degli Studi di Padova, I-35131 Padova, Italy*
[5]*INFN, Sezione di Padova, I-35131 Padova, Italy*
[6]*The Niewodniczanski Institute of Nuclear Physics, PAN, 31-342 Krakow, Poland*
[7]*Institut für Kernphysik, Universität zu Köln, D-50937 Köln, Germany*
[8]*INFN, Laboratori Nazionali di Legnaro, Legnaro I-35020, Italy*
[9]*Department of Physics, Royal Institute of Technology, SE-10691 Stockholm, Sweden*
[10]*Centre de Spectrométrie Nucléaire et de Spectrométrie de Masse CSNSM, CNRS/IN2P3, and Université Paris-Sud, F-91405 Orsay Campus, France*
[11]*IFIC, CSIC-Universitat de València, E-46980 València, Spain*
[12]*Department of Physics, University of Oslo, N-0316 Oslo, Norway*
[13]*Instituto de Estructura de la Materia, CSIC, Madrid, E-28006 Madrid, Spain*
[14]*Department of Physics, University of Surrey, Guildford GU2 7XH, United Kingdom*
[15]*STFC Daresbury Laboratory, Daresbury, Warrington WA4 4AD, United Kingdom*
[16]*Laboratorio de Radiaciones Ionizantes, University of Salamanca, E-37008 Salamanca, Spain*
[17]*Department of Physics and Astronomy, Uppsala University, SE-75120 Uppsala, Sweden*
[18]*Université de Lyon, Université Lyon 1, CNRS-IN2P3, Institut de Physique Nucléaire de Lyon, F-69622 Villeurbanne, France*
[19]*Institut de Recherche sur les lois Fondamentales de l'Univers IRFU, CEA/DSM, Centre CEA de Saclay, F-91191 Gif-sur-Yvette Cedex, France*

(Received 9 December 2014; revised manuscript received 20 January 2015; published 24 February 2015)

2^+ and 1^- states in ^{90}Zr were populated via the (^{17}O,^{17}O$'\gamma$) reaction at 340 MeV. The γ decay was measured with high resolution using the AGATA (advanced γ tracking array demonstrator array). Differential cross sections were obtained at few different angles for the scattered particle. The results of the elastic scattering and inelastic excitation of 2^+, 3^-, and 1^- states are compared with distorted-wave Born approximation (DWBA) calculations, using both the standard collective form factor and a form factor obtained by folding microscopically calculated transition densities. This allowed to extract the isoscalar component of the 1^- state at 6.424 MeV. The comparison of the present (^{17}O,^{17}O$'\gamma$) data with existing (γ,γ') and (p,p') data in the corresponding region of the γ continuum (6–11 MeV), characterized by a large $E1$ component, shows completely different behaviors of the cross section as a function of the nuclear excitation energy. The comparison of the data with DWBA calculations suggests a decrease of the isoscalar strength in the cross section with increasing excitation energy.

DOI: 10.1103/PhysRevC.91.024323 PACS number(s): 24.30.Cz, 24.10.Eq, 25.70.Bc, 27.60.+j

I. INTRODUCTION

Particular attention has been given in the past few years to detailed investigations of the properties of the dipole strength around the particle emission threshold. This $E1$ strength is denoted as pygmy dipole resonance (PDR) and is found to be particularly sizable in neutron-rich nuclei [1–4]. The properties of the PDR strength are connected to the properties of the neutron skin which are used to constrain the equation of state of neutron-rich matter [5–7]. A key issue for the interpretation of the nature of the PDR states is the determination of their isospin character. In this connection extensive work [8–13] was made using the (α,α') reaction, having a strong isoscalar character, and the general result is the presence of different excitation

*angela.bracco@mi.infn.it
†Present address: CEA, Centre de Saclay, IRFU/Service de Physique Nucléaire, F-91191 Gif-sur-Yvette, France.
‡Present address: Grand Accélérateur National d'Ions Lourds (GANIL), CEA/DSMCNRS/IN2P3, F-14076 Caen Cedex 5, France.
§Present address: Grand Accélérateur National d'Ions Lourds (GANIL), CEA/DSMCNRS/IN2P3, F-14076 Caen Cedex 5, France.
‖Present address: Department of Physics, University of Oslo, N-0316 Oslo, Norway.
¶Present address: RIKEN Nishina Center, 2-1 Hirosawa, Wako, 351-0198 Saitama, Japan.

pattern as compared with that of the (γ,γ') reaction. More recently, experiments performed for the nuclei ^{208}Pb [14], ^{124}Sn [15], and ^{140}Ce [16] to study the $E1$ and $E2$ transitions in the region 4–9 MeV have shown that the $(^{17}\mathrm{O},^{17}\mathrm{O}'\gamma)$ reaction is a good tool to investigate the isospin properties of these states. Indeed, this reaction enhances the excitation of the isoscalar component of states populated with it. The isospin properties of 1^- and 2^+ states in ^{208}Pb and ^{124}Sn were deduced from the comparison with (γ,γ') data. To obtain a more general understanding of the 2^+ and 1^- states in moderately neutron-rich nuclei, the investigation of the nucleus ^{90}Zr is very relevant. For this nucleus, characterized by neutron shell and proton subshell closures, (γ,γ') data are available [17] and a measurement with (p,p') with polarized protons was recently made at 0° to excite nuclear states predominantly by Coulomb excitation [18]. Furthermore, the rather high value of the neutron separation energy (11.97 MeV) in ^{90}Zr makes it possible to investigate a large region of excitation energy via γ decay.

In this paper we report on results of an experiment made to study the properties of 2^+ and 1^- states in ^{90}Zr using the $(^{17}\mathrm{O},^{17}\mathrm{O}'\gamma)$ reaction. For the discussion of the results it is very important to make model predictions using $B(E1)$ and $B(E2)$ data obtained with the (γ,γ') [17] and (p,p') [18] reactions. We anticipate here that, although the present $E1$ data have limited statistics above 6.5 MeV (and thus are integrated in 0.5-MeV bins), the corresponding findings are interesting also in view of possible future investigations with high statistics and using different probes. For the very intense ground-state $E1$ transition at 6.424 MeV, it was possible to extract by a theoretical analysis the isoscalar component of this excited state. For the 2^+ states new γ decays were found and comparisons of their measured excitation cross sections with predictions indicate that surface properties could vary from state to state.

II. THE EXPERIMENT

The inelastic scattering of ^{17}O ions at bombarding energy of 20 MeV/u was measured recently to study pygmy states in the ^{208}Pb [14] and ^{124}Sn [15] nuclei. Previously, the same reaction was used at 22 MeV/u to study the γ decay of the isoscalar giant quadrupole resonance (ISGQR) of ^{208}Pb [19] and at 84 MeV/u [20,21] to study giant resonances, in particular the giant dipole resonance (GDR), in ^{208}Pb, ^{120}Sn, ^{90}Zr, and ^{60}Ni. The choice of ^{17}O, instead of the most abundant ^{16}O, is related to the fact that one can reduce considerably the background from the decay of excited states of the projectile by using ^{17}O. Indeed, ^{17}O has a rather small neutron separation energy ($S_n = 4.1$ MeV) and thus the identification in the experiment of ^{17}O ions as scattered particles assures excitation of the target nucleus when the transferred excitation energy is larger than 4 MeV.

In the present experiment a beam of ^{17}O ions at a bombarding energy of 340 MeV was provided by the Tandem-ALPI accelerator complex of the Legnaro National Laboratories of INFN at Legnaro (Italy). A self-supporting target of ^{90}Zr was used with a thickness of 2 mg/cm^2. The scattered ions were detected, as coincidences and scaled-down singles, using two segmented silicon telescopes (pixel type) placed at approximately 9° and symmetrically with respect to the beam direction. These telescopes are prototypes built for the TRACE project [22]. Each used Si detector had an horizontal size of 20 mm and a vertical size of 50 mm and included 60 pixels each with an area of 4 × 4 mm. For these Si detectors *ad hoc* electronic adapter boards were built which selected the 32 pixels closest to the beam direction. The front face surfaces of the electronically connected pixels formed approximately a disk in the plane perpendicular to the beam at distance of 8 cm from the target center. The two ΔE-E silicon telescopes each consisted of a thin "ΔE" detector placed in front of a thick "E" detector. The ΔE detectors were 200 μm thick, producing an energy loss of about 70 MeV for ^{17}O ions at 340 MeV. The E detectors were 1 mm thick and this thickness was sufficient to stop the ^{17}O ions completely. The thresholds of the Si detectors were such that a large fraction of events corresponding to protons and α particles were rejected. The overall energy resolution was typically around 0.3% at 340 MeV.

The detection of γ rays, emitted in coincidence with events measured in the Si telescopes, was performed with the advanced γ tracking array (AGATA) demonstrator. AGATA is a high-purity germanium (HPGe) detector array of new generation making it possible to use the techniques of pulse-shape analysis and of γ-ray tracking [23,24]. At the time of this experiment the AGATA demonstrator consisted of three triple clusters of HPGe detectors and was placed 13.5 cm from the target covering an angular range in θ from 100° to 150° (relative to the beam direction). The segmentation of the HPGe detectors made it possible to define the direction of the γ-ray emission with a precision of 1°. The AGATA detection efficiency was deduced from measurements with radioactive γ sources and by simulations performed with the computer code GEANT4 [25,26] including the geometrical configuration of this particular experiment.

The collected data that were analyzed in this work were coincidences of at least one hit of the Si telescopes with at least one γ ray in AGATA. With the used Si telescopes, it was possible using the E-ΔE correlation to identify the inelastically scattered ions in the presence of several other reaction channels. Moreover, the pixels inside the telescopes were used to measure the correlation between the direction of the γ ray with the beam and with the velocity of the recoiling nuclei, the latter deduced from two-body kinematics. The correlation with the beam direction was particularly useful to check with rather good precision the angular position of each pixel. For this purpose the Doppler shift of the 6.13-MeV γ-ray transition of the ^{16}O nucleus was examined for each pixel. The ^{16}O ions were well identified from ^{17}O ions in the E-ΔE correlation of the collected events. The 6.13-MeV γ rays coming from a source moving with the beam velocity, corresponding to a β of 0.2, resulted in being the most sensitive, among the available transitions, to the Doppler shift correction. Because of the nonspherical geometry of the Si detector array, each pixel in a given vertical row has a specific value of the polar angle θ depending on its distance from the horizontal line passing through the beam center. This resulted in up to eight different angular points, from 7.9° to 12.5° in the laboratory (9.4°–14.9° in the center of mass), for elastic scattering where the highest statistics was available. The

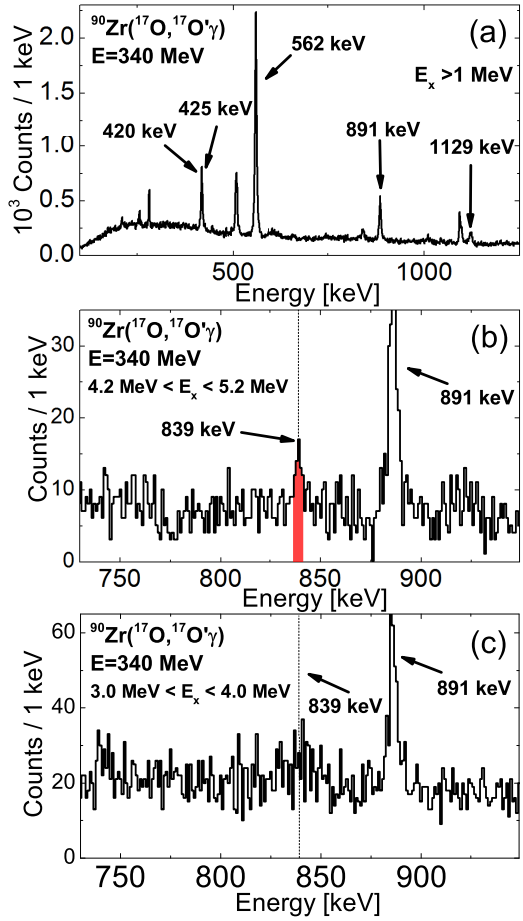

FIG. 1. (Color online) (Top) γ-ray energy spectrum in the 100–1250-keV interval, measured with the AGATA array and corresponding to the ^{17}O scattering channel with the additional gating condition for selecting the kinetic energy loss of the scattered ions corresponding to $E_X > 1$ MeV. (Middle) γ-ray energy spectrum in the 730–950-keV interval, measured with the AGATA array, corresponding to the ^{17}O scattering channel with a gate at $E_x = 4.7$ MeV (±0.5 MeV). (Bottom) Same as above; in this case the gate is at $E_x = 3.5$ MeV (±0.5 MeV).

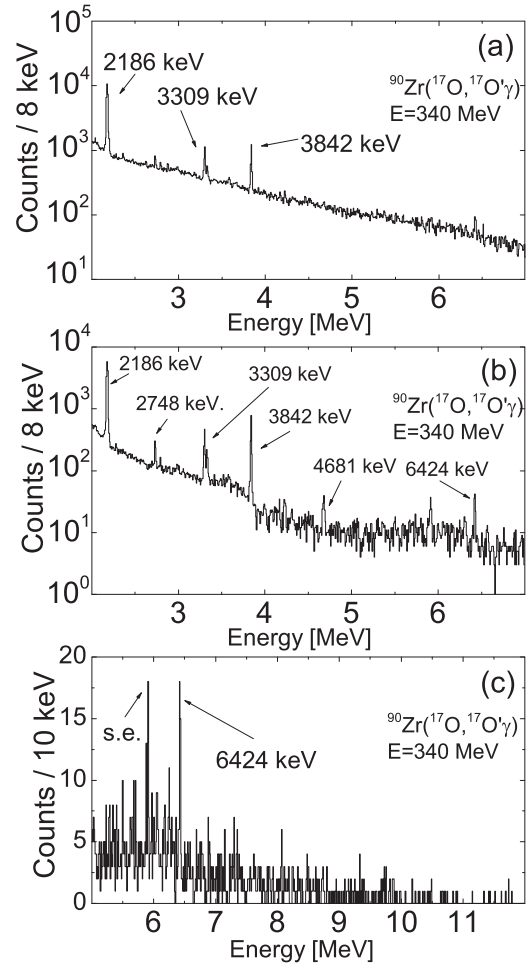

FIG. 2. (Top) γ-ray energy spectrum in the 2–7-MeV interval, measured with the AGATA array and corresponding to the ^{17}O scattering channel. (Middle) γ-ray energy spectrum in the same interval, corresponding to the ^{17}O scattering channel with the additional condition of selecting the deexciting transitions to the ground state. (Bottom) γ-ray energy spectrum in the 5–12-MeV interval, measured with the AGATA array, corresponding to the ^{17}O scattering channel, selecting the deexciting transitions to the ground state and with the additional condition on the angle between the emitted γ ray and the recoil direction which enhances the $E1$ component. The peak corresponding to the single escape (s.e.) from pair production for the 6424-keV transition is indicated with an arrow.

average beam current was around 0.5 pnA, a value that was imposed by the limit of counting rate for the γ-ray detectors.

Several γ-ray energy spectra of AGATA were constructed from the data under different conditions for the detected scattered ^{17}O ions. Figure 1 shows three particular γ-ray energy spectra. The spectrum in the top panel refers to transition energy in the interval 0.1–1.25 MeV and was obtained with a condition on the energy of the scattered ^{17}O particles corresponding to excitation energies of ^{90}Zr larger than 1 MeV. The most intense peaks indicated with arrows in the spectrum correspond to well-known transitions, which are the 420-keV transition (decay from the 4^- state at 2.739 MeV to the 5^- state at 2.319 MeV), the 425-keV transition (decay from the 2^+ state at 2.186 MeV to the 0^+ state at 1.76 MeV), the 562-keV transition (decay from the 3^- state at 2.747 MeV to the 2^+ state at 2.186 MeV), the 890-keV transition (decay from the 4^+ state at 3.0769 MeV to the 2^+ state at 2.1869 MeV), and the 1129-keV transition (decay from the 6^+ state at 3.448 MeV to the 5^- state at 2.319 MeV). One important point in connection with the discussion of 2^+ states is the identification of their γ-decay branches to excited states. In most cases only few counts are expected for γ-ray transitions with $E_\gamma < 1$ MeV from 2^+ states to low-lying excited states. These are difficult to identify because they are in the region where the Compton background is rather high. Therefore, we have examined γ-ray spectra with conditions on the kinetic energy of the scattered ions (corresponding to conditions on the nuclear excitation energy) and found that the spectrum obtained with a gate at $E_x = 4.7$ MeV (±0.5 MeV) contains a transition of interest for the decay of the 2^+ state at 4.681 MeV. This spectrum is shown in the middle panel of Fig. 1 with an

expanded scale (0.73–0.95 MeV). There a peak at 839 keV is clearly visible. In contrast, in the spectrum obtained with a condition on the kinetic energy loss of the scattered ions corresponding to $E_X = 3.5$ MeV (± 0.5 MeV), shown with the same expanded scale in the bottom panel of Fig. 1, such 839-keV transition cannot be seen. The 839-keV transition is then tentatively assigned as deexcitation from the 4.681-MeV state to the 3.842-MeV state (see Fig. 4).

The γ-ray energy spectrum in the energy interval 2–7 MeV obtained without any condition on the excitation energy of the ^{90}Zr nucleus is shown in the top panel of Fig. 2. Several peaks are present in this spectrum that are associated with transitions of different multipolarity. In particular, one sees the transitions to the ground state from three 2^+ states at energy of 2.186, 3.309, and 3.842 MeV and the ground-state transition from the 3^- state at 2.748 MeV. These transitions and others are seen much better in the middle-panel spectrum that was obtained requiring the γ-ray energy be equal, within the energy resolution of the charged-particle telescopes, to the excitation energy of the nucleus. This condition makes it possible to select direct decays to the ground state. In this spectrum the ground-state transitions from the 2^+ at 4.681 MeV and from the 1^- at 6.424 MeV are also visible. The γ-ray spectrum associated with the angles in which the dipole emission is maximized as compared with the quadrupole emission is shown in the bottom panel of Fig. 2. There one can note that for the many transitions of $E1$ type known from the (γ,γ') experiment [17], one can see well only the one at 6.424 MeV, while the other transitions at $E_\gamma > 6.5$ MeV have only a few counts. Therefore, the identification of each specific transition being very difficult, the data at $E_\gamma > 6.5$ MeV were integrated over wide bins as discussed in the following section.

To deduce the dominant multipolarity of the γ transitions in the region 6.5–10 MeV we have integrated their yields in two angular intervals, 100°–125° and 125°–150° (angles relative to the beam direction). We deduced the yield ratio $Y_R = Y(125°–150°)/Y(100°–125°)$ in that transition energy interval and we compared it with the values measured for the known 1^- state at 6.424 MeV and for the known 2^+ states at 2.186, 3.309, and 3.842 MeV. These Y_R values are shown in Fig. 3 together with two colored bands, one for the $E1$ transitions (the blue one) and one for $E2$ transitions (the red one), giving the average value and average uncertainty. For transitions at $E_\gamma > 6.5$ MeV two Y_R points are shown one for the 6.5–8-MeV interval and the other for the 6.5–10-MeV interval. One can note that the Y_R values for transitions in the 6.5–10-MeV interval are very similar to the Y_R (6.424) point. In addition, the Y_R values for $E2$ transitions are different than those for $E1$ transitions. From this discussion one can infer a dominant $E1$ character to transitions in the 6.5–10-MeV interval, although the presence of $M1$ and $E2$ transitions cannot be fully excluded.

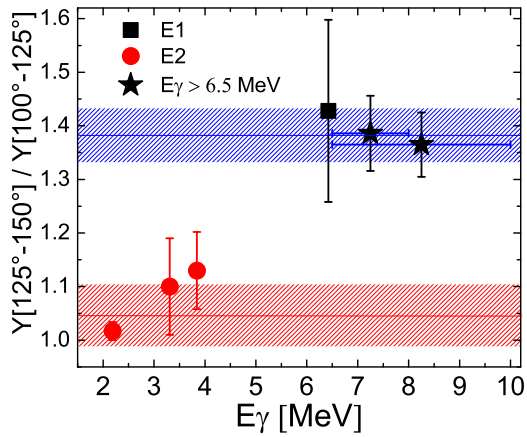

FIG. 3. (Color online) The yield ratio $Y_R = Y(125°–150°)/Y(100°–125°)$ is shown for the known 1^- state at 6.424 MeV and for the known 2^+ states at 2.186, 3.309, and 3.842 MeV together with that of continuous transitions in the energy interval 6.5–10 MeV. The error bars are statistical uncertainties. The two colored bands are one for the $E1$ transitions (the blue one) and the other for $E2$ transitions (the red one). They give the average Y_R values for $E1$ and $E2$ transitions and the average uncertainty.

III. THE POPULATED LEVELS

In Fig. 4 the part of level scheme of the ^{90}Zr nucleus with the γ transitions observed in the present experiment is shown. The γ transitions populated with this experiment are well known with the exception of the transitions at 839 keV and 4.681 MeV originating from the 2^+ state at 4.681 MeV. While this 4.681-MeV state was seen before and identified as 2^+, its γ decay was not previously known. Based on excitation cross-section arguments (see below) we concluded for the 4.681 MeV level that, in addition to these two identified decay

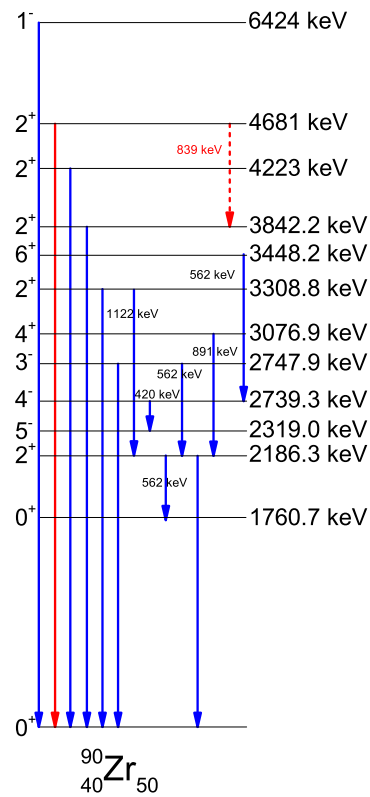

FIG. 4. (Color online) The level scheme of ^{90}Zr relevant to this measurement, showing the γ transitions observed in the present work.

branches, other sizable branches might exist. These could feed, for example, other 2^+ states at lower energies. Moreover, these transitions are expected to have energies mainly below 2 MeV and a number of counts smaller than the Compton background present in the γ-ray spectrum at $E_\gamma < 2$ MeV. Therefore, we could not identify them and consequently the population cross section of the 4.681-MeV state could not be inferred from the present data.

The following analysis of the cross section for the population of various excited states is therefore restricted to the states for which the γ-decay branching ratios are summing to 100% of the intensity (as known from previous works). The results and discussions concerning elastic scattering and excitation cross section for the 2^+, 1^-, and 3^- states in ^{90}Zr seen in this experiment are given in the following sections.

IV. ELASTIC SCATTERING AND THE 3⁻ STATE

The first step of the analysis of the measured cross sections concentrated on the elastic scattering channel, which was also measured in this experiment. A calculation for the elastic scattering differential cross section (^{17}O,^{17}O) was performed within the optical model approach using the FRESCO [27,28] code. This code was used for all the DWBA calculations given in this paper. A good reproduction of the data was obtained with the following optical model parameters for Woods-Saxon potentials: $V = 40.0$ MeV, $W = 26$ MeV (with V and W the depth of the real and imaginary potentials, respectively), $r_v = r_W = 1.15$ fm, $a_V = a_W = 0.671$ fm (the radii and diffuseness of the real and imaginary parts), and $r_C = 1.20$ fm (the Coulomb radius parameter). The overall experimental normalization was obtained by normalizing the measured elastic scattering yield at $\theta = 9.4^\circ$ in the center-of-mass frame of reference to the calculated cross section at the same angle. The normalization value at $\theta = 9.4^\circ$ accounts for the combined effect of the integrated current, target thickness, and effective solid angles. The comparison of the experimental elastic scattering data with the corresponding optical model predictions is shown in the top panel of Fig. 5. The experimental points are well reproduced by calculations over the entire angular interval.

The analysis of cross sections for excited states uses the optical model parameters deduced from elastic scattering and as a normalization factor the same overall normalization deduced from the elastic scattering multiplied with the γ-ray detection efficiency (e.g., at 2.186 MeV is 2.9%). Indeed for the comparisons of excited-state data with the corresponding DWBA predictions no further normalization was made. In the bottom panel of Fig. 5 the data for the excitation cross section of the 3^- state at 2.748 MeV are shown in comparison with a DWBA calculation. For the experimental data it has to be specified that the 3^- state decays either directly to the ground state or to the first 2^+ at 2.186 MeV. Therefore, the total intensity is the sum of the two contributions from the transitions at 2.748 and 0.562 MeV. For the DWBA calculation the known value of the $B(E3)\uparrow = 27\,000\ e^2\ \mathrm{fm}^6$ was used together with the collective form factor describing surface vibrational states. The ratio of the neutron and proton transition matrix elements was assumed to be $M_n/M_p = N/Z$. This calculation reproduces rather well the data for all the measured angles.

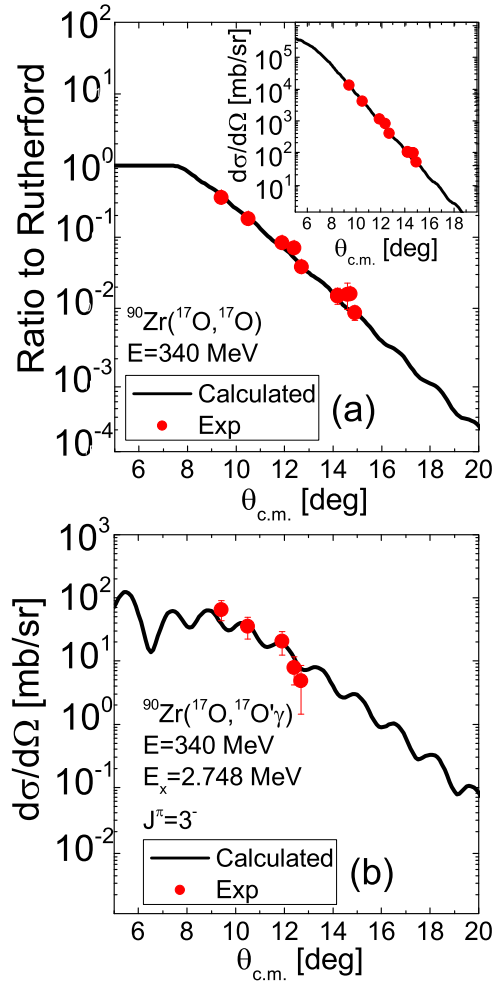

FIG. 5. (Color online) (Top) ^{90}Zr(^{17}O,^{17}O)^{90}Zr elastic-scattering differential cross section in the center-of-mass frame measured at $E_{\mathrm{beam}} = 340$ MeV is shown in the inset of the figure. Data and calculations divided by the Rutherford cross section are displayed in the panel. (Bottom) Measured differential cross section ^{90}Zr(^{17}O,^{17}O$'\gamma$)^{90}Zr* at the same bombarding energy for the 3^- state at 2.748 MeV. The error bars shown with the data points represent the statistical error. The solid line curves are the predictions, described in the text, obtained within the optical model and the DWBA approach.

V. THE 2⁺ STATES

In the present experiment, five 2^+ excited states were populated, at 2.186, 3.309, 3.842, 4.223, and 4.681 MeV, respectively. However, the DWBA analysis for their excitation cross section was performed only for the first three of these 2^+ states. For the last two 2^+ states not all the γ-decay branches were measured or were known and thus we did not have 100% of the γ strength as required for the DWBA analysis.

The differential cross-section data for the excitation of the first collective 2^+ state at 2.186 MeV are shown in panel (a) of Fig. 6. The corresponding DWBA calculation includes the

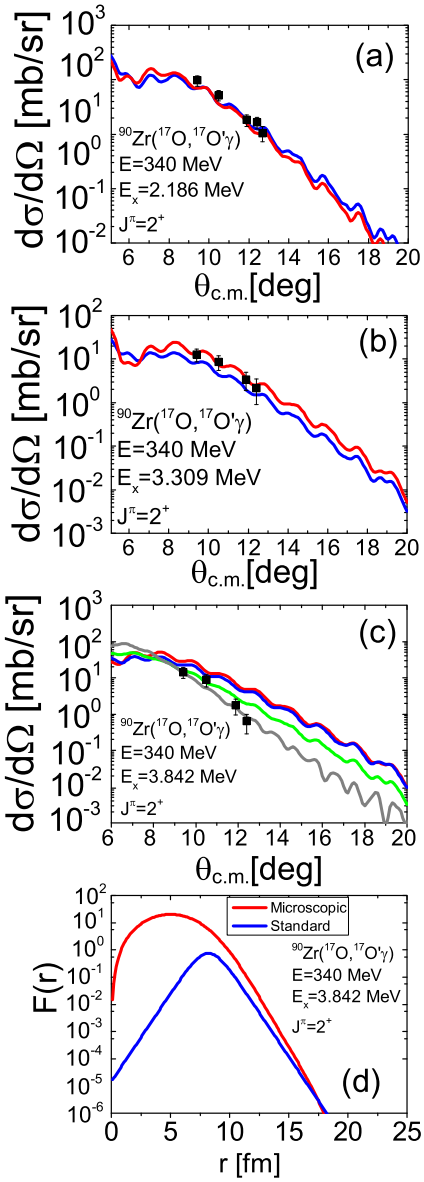

FIG. 6. (Color online) Inelastic scattering cross section ^{90}Zr(^{17}O,^{17}O$'\gamma$)^{90}Zr* at 340 MeV for the 2^+ states 2.186 MeV (a), 3.309 MeV (b), 3.842 MeV (c) (black solid squares). The error bars are the statistical errors. The lines show DWBA calculations. The blue solid curves are the calculations with the standard phenomenological form factor [displayed in panel (d), blue line]. The red solid lines include the nuclear contribution calculated with the microscopic form factor shown in panel (d) (red line; see text) and derived with the transition density shown in the bottom panel of Fig. 7. For the case of the 3.842-MeV state [panel (c)] DWBA calculations performed with the standard phenomenological form factor but considering $M_n/M_p = 0.1 * N/Z$ (green line) are displayed. The gray curve represents the calculation performed considering only the Coulomb excitation.

adopted [29] $B(E2)\uparrow = 653\ e^2\ \mathrm{fm}^4$ value, uses the vibrational collective form factor, and assumes that the ratio of the neutron and proton transition matrix elements is $M_n/M_p = N/Z$ (i.e., pure isoscalar). It is clear from the comparison of the data with the calculation [the black line in panel (a) of Fig. 6] that the deformed potential model is able to reproduce well the experimental data. Also in case of the higher lying state at 3.309 MeV a good agreement is found between data and predictions, corresponding to a calculation performed using the adopted $B(E2)\uparrow = 78.4\ e^2\ \mathrm{fm}^4$ value and $M_n/M_p = N/Z$ (i.e., pure isoscalar). These calculated cross sections are shown with the black line in panel (b) of Fig. 6.

In contrast with the case of the first two 2^+ states, for the 3.842-MeV state it is not possible to reproduce the data with calculations using the standard deformed potential model approach. A calculation for this state was made using the adopted $B(E2)\uparrow = 224\ e^2\ \mathrm{fm}^4$ value and the condition $M_n/M_p = N/Z$. Indeed, the slope of the data and of the DWBA calculation as a function of angle of the scattered particles are different.

Additional calculations were performed for which the adopted radial form factor is of microscopic type. The radial form factor employed in the calculations was built up with the double folding procedure by using the microscopic random-phase approximation (RPA) transition densities as described in Ref. [30]. This microscopic nuclear form factor is shown with a red line in the bottom panel of Fig. 6 in comparison with the nuclear part of the collective form factor used for surface vibrational states (blue line). Also in this case the DWBA calculation [for which the $B(E2)\uparrow = 224\ e^2\ \mathrm{fm}^4$ value was also used] does not reproduce the cross-section data. Note that for this comparison of the data with DWBA predictions no further normalization was made. The almost identical DWBA predictions found when using either the macroscopic or the microscopic nuclear form factor reflect the fact that the reaction (^{17}O,^{17}O$'\gamma$) is probing mainly the nuclear surface where the two nuclear form factors are very similar. For the sake of completeness, calculations adopting microscopic form factors [very similar to that of Fig. 6(d)] and scaled according to the adopted $B(E2)$ values were also made for the 2.186- and 3.309-MeV 2^+ states. As one can see from the first two panels of Fig. 6, where these calculations are shown with the red lines, a reasonable account of the experimental data is obtained. To investigate further the discrepancy found between data and calculations in the case of the 3.842-MeV state, a DWBA calculation was also performed with the standard phenomenological form factor and assuming $M_n/M_p = 0.1 * N/Z$. This prediction is shown in panel (c) of Fig. 6 with the green line. One sees clearly that by lowering the nuclear contribution the associated calculations get closer to the experimental points. We also show in panel (c) of Fig. 6 a gray curve which corresponds to a calculation performed considering only the Coulomb excitation contribution. This calculation is the one that better reproduces the data and the reason for this can be related to the particular nature of this state. As stated in Ref. [29], this state was described as having a strong four-quasiparticle component and therefore cannot be populated by a one-step process as that assumed within the DWBA approach. However, a calculation that uses of the measured $B(E2)$ value ensures the correct direct excitation via the Coulomb potential while the nuclear potential does not play a significant role in the direct excitation process of such a complex excitation mode.

VI. THE 1⁻ STATES

The present reaction populates very well the 1^- state at 6.424 MeV, for which the γ transition to the ground state is well identified in the γ-ray spectrum measured with AGATA. For this state the angular distribution was obtained, as shown in the top panel of Fig. 7. The DWBA calculation for this state, based on the adopted $B(E1)\uparrow = 0.018\ e^2\ \mathrm{fm}^2$ value and with the standard form factor used for isovector dipole states (as, for example, the GDR), is shown as a black solid line in Fig. 7. As one can see, this calculation accounts only for a rather small fraction of the measured yield. In this calculation the Coulomb part is the dominant one and it is fixed by the known $B(E1)\uparrow$ value deduced from the (γ,γ') data of Ref. [17]. It is clear that the nuclear part is not well described by the standard distorted potential approach in the case of this 1^- state. Similarly to what was done in recent analyses of 1^- states in ^{208}Pb [14] and ^{124}Sn [15], also for the 1^- state at 6.424 MeV in ^{90}Zr a calculation was performed using a microscopically

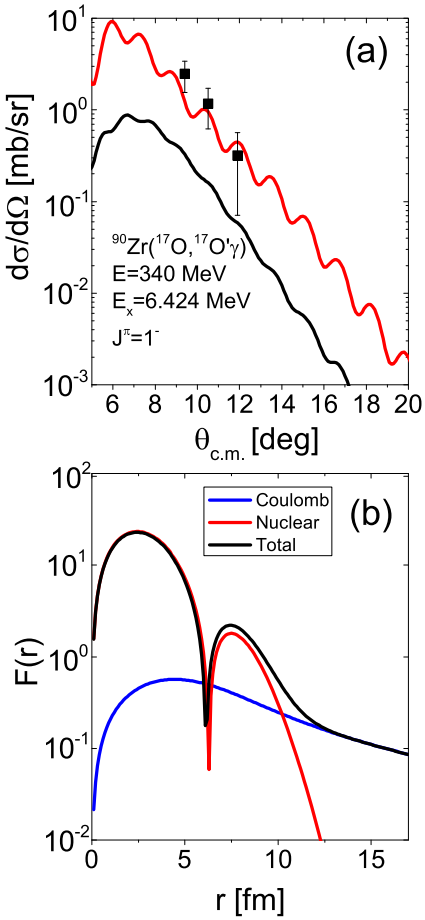

FIG. 7. (Color online) (Top) Inelastic scattering cross section ^{90}Zr(^{17}O,^{17}O′γ)^{90}Zr* at 340 MeV for the 1^- state 6.424 MeV. The error bars are the statistical errors. The lines show DWBA calculations. The black solid curve represents the calculations with the standard phenomenological form factor. The red solid line includes the nuclear contribution calculated with the microscopic form factor shown in the bottom panel (see text) and derived with the transition density shown in the Fig. 8.

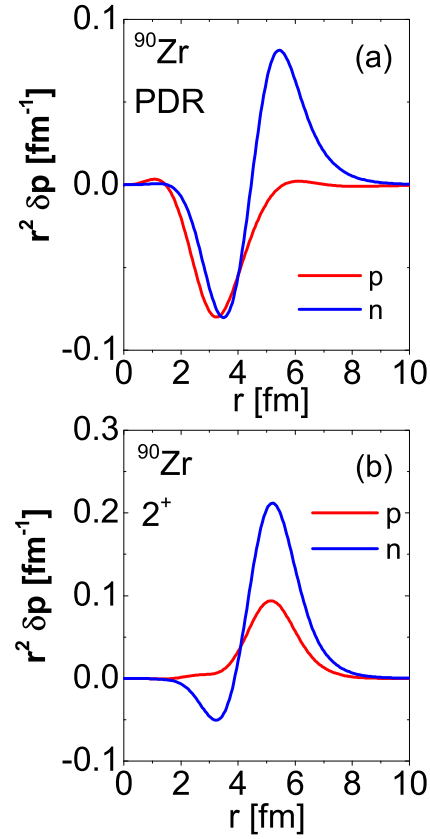

FIG. 8. (Color online) Transition densities for protons (red line) and neutrons (blue line) used to derive the form factors for the microscopic calculations for the 1^- pygmy states (top panel) and 2^+ states (bottom panel).

calculated form factor. The form factor was calculated by a double folding procedure with a M3Y nucleon-nucleon interaction. The ground-state density and the transition density were obtained with Hartree-Fock plus RPA calculations with a SGII (Sagawa-Giai II, see Ref. [30]) interaction. The proton and neutron transition densities for a 1^- state are shown in Fig. 8 (in the top panel). In the bottom panel of Fig. 8 the proton and neutron transition densities for a 2^+ state are also displayed. These transition densities show the typical behavior of pure isoscalar states. For the 2^+ state, proton and neutron transition densities oscillate in phase. Instead, for the 1^- state proton and neutron transition densities are characterized by an oscillation in phase inside the nucleus and by a concentration of only neutron strength at the surface. This is the typical behavior of a pygmy state characterized by a concentration of neutron strength at the surface. The corresponding form factors are shown in the bottom panels of Figs. 6 and 7, from which one can appreciate the different structure of the two form factors. In particular, the one corresponding to the low-lying dipole (PDR) state shows a positive interference, between Coulomb and nuclear components, inside the nucleus and a negative one at the surface. This is attributable to the presence of a node in the isoscalar transition density of the PDR state. One can note that for the 1^- state the form factor from the microscopic description is very different at the nuclear surface as compared

with that based on the distorted potential. The microscopic calculation corresponds to a fraction of 2.4% of the isoscalar energy-weighted sum rule (EWSR) strength. By fitting the 6.424-MeV data with calculations a value of 2.17% of EWSR strength for the isoscalar dipole was found.

The ^{90}Zr(^{17}O,^{17}O$'\gamma$)^{90}Zr* data at $E\gamma > 6.5$ MeV are expected to have a dominant $E1$ character. This is based on three different considerations. The first is that the (γ,γ') data from Ref. [17] show the presence of many dipole states with a large fraction having electric character as also deduced from (p,p') data from Ref. [18]. The second consideration is that the $(^{17}\mathrm{O},^{17}\mathrm{O}'\gamma)$ reaction similarly to the $(\alpha,\alpha'\gamma)$ reaction populates predominantly natural parity states such as 1^- and 2^+. The third is that the intensity ratio Y_R in two angular intervals 125°–150° and 100°–125° (see Fig. 3) is consistent

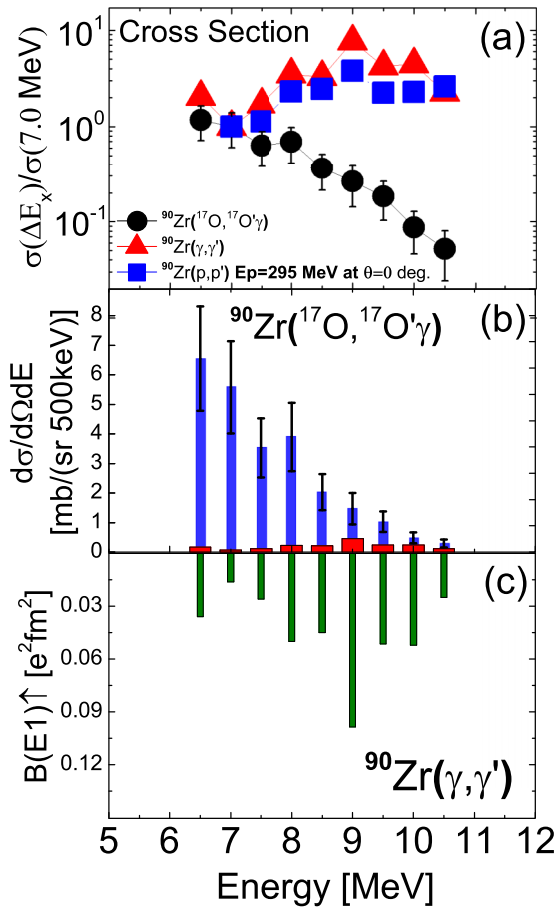

FIG. 9. (Color online) (Top) The quantity $\sigma_R = \sigma(E_x)/\sigma(7\,\mathrm{MeV})$ in 0.5-MeV bins as a function of excitation energy, for the reactions $(^{17}\mathrm{O},^{17}\mathrm{O}'\gamma)$ (black solid circles), and deduced from (γ,γ') data (red triangles) [17] and from (p,p') $E1$ data (blue solid squares) from Ref. [18]. The lines are to guide the eyes and the error bars the statistical uncertainties. (Middle) The measured differential cross section at the average angle 10.5° for γ transitions in 0.5-MeV bins is displayed with blue bars. The red bars give calculated DWBA cross-section predictions assuming $E1$ and using the $B(E1)\uparrow$ values from (γ,γ') [17] and standard form factors (see text). (Bottom) Electromagnetic reduced $E1$ transition strength deduced from the (γ,γ') data of Ref. [17], assuming $E1$ transitions.

with γ transitions of dominant $E1$ character at $E_\gamma > 6.5$ MeV. The states at $E_x > 6.5$ MeV in ^{90}Zr are weakly populated by the $(^{17}\mathrm{O},^{17}\mathrm{O}'\gamma)$ reaction and because of low statistics the cross-section data for $E_\gamma > 6.5$ MeV were binned at 0.5 MeV. These cross sections are shown in the middle panel of Fig. 9 with blue bars together with DWBA calculations using the standard deformed potential form factors (red bars). These DWBA calculations were made using for the quantity $B(E1)$ the experimental values deduced from the (γ,γ') experiment of Ref. [17] and which are given in the bottom panel of Fig. 9. Note that in all these calculations (with the standard deformed potential form factors) the Coulomb component is dominant. It is clear that only at around 10–11 MeV are the data somewhat reasonably reproduced by the calculations. In this 10–11-MeV region the calculated transition densities reported in Ref. [17] suggest that the $E1$ mode is of GDR type, namely with protons and neutrons out of phase and covering the same spatial extension. Altogether, this comparison between the measured and calculated cross sections shows the presence of an isoscalar component in the cross section decreasing in strength as the excitation energy of the nucleus increases.

It is interesting to compare for this nucleus the relative behavior of the cross sections measured at $E_x > 6.5$ MeV with the $(^{17}\mathrm{O},^{17}\mathrm{O}'\gamma)$, the (γ,γ'), and the (p,p') reactions. For this purpose, the quantity $\sigma_R = \sigma(E_x)/\sigma(7\,\mathrm{MeV})$, where $\sigma(E_x)$ is the cross section at excitation energy E_x, has been evaluated for these three reactions. This quantity (equal to 1 at 7 MeV and in all cases given in bins 0.5 MeV wide) is shown in the top panel of Fig. 9 for the three reactions. The error bars in the cases of the (γ,γ') and (p,p') data are smaller than the symbols and for $(^{17}\mathrm{O},^{17}\mathrm{O}'\gamma)$ data reflect the statistical uncertainties. A strong increase of these relative cross sections in the excitation energy interval 6.5 to 11 MeV is observed for the (γ,γ') and (p,p') data, while a strong decrease is evident in the $(^{17}\mathrm{O},^{17}\mathrm{O}'\gamma)$ data. More data with higher statistics, smaller energy binning and obtained with other types of reactions are needed to get a better insight into the nature of 1^- states, particularly in the energy region where a transition between pygmy states and GDR type states occurs.

VII. SUMMARY

The present experiment has studied the $(^{17}\mathrm{O},^{17}\mathrm{O}'\gamma)$ inelastic scattering reaction at 340 MeV on the ^{90}Zr nucleus. The measured cross section for the elastic scattering, for the first two 2^+ states and for the 3^- state are well reproduced by the DWBA approach using the deformed collective form factor and for the ratio of the neutron and proton transition matrix elements the expression $M_n/M_p = N/Z$ (i.e., pure isoscalar). For the 2^+ state at 3.842 MeV some evidence is found for a different shape of the transition density at the nuclear surface as compared with the other two 2^+ states. For the 2^+ state at 4.681 MeV the γ transition to the ground state and the one populating the state at 3.842 MeV are seen for the first time. The strong $E1$ transition from the 6.424-MeV 1^- state was analyzed using the standard collective model form factor and a microscopic form factor, only the latter reproducing the data. From this analysis it was found that the 1^- state at 6.424 MeV has a dominant isoscalar component

and has a character typical of pygmy states. In addition, it exhausts 2.17% of the isoscalar dipole EWSR strength. At $E_\gamma > 6.5$ MeV the present (^{17}O,^{17}O$'\gamma$) data appear to have a dominant $E1$ component and because of the limited statistics the cross sections were deduced for bins 0.5 MeV wide. The quantity $\sigma_R = \sigma(E_x)/\sigma(7\ \text{MeV})$ was evaluated for the present data and for the (γ,γ') and (p,p') data (Refs. [17] and [18]). The trend of $\sigma_R = \sigma(E_x)/\sigma(7\ \text{MeV})$ as a function of excitation energy is very similar for the (γ,γ') and (p,p') reactions, while it is different for the (^{17}O,^{17}O$'\gamma$) reaction. Altogether this experiment suggests the presence of an isoscalar component at $E_\gamma > 6.5$ MeV, which decreases with increasing excitation energy. Further work on the ^{90}Zr nucleus should be made, keeping in mind that this nucleus offers the possibility to investigate γ decay from discrete dipole states in a wide region of excitation energy up to approximately 12 MeV. New experiments providing more statistics at excitation energies larger than 6.5 MeV are necessary to shed more light on the problem of the nature of pygmy states in this nucleus. In addition, it will be important to use other probes such as the scattering of α particles.

ACKNOWLEDGMENTS

We acknowledge support from several grants. From Poland, we received Grants No. DPN/N190/AGATA/2009 No. 2011/03/B/ST2/01894, No. 2013/09/N/ST2/04093, and No. 2013/08/M/ST2/00591; from Italy, we received support from INFN; One of the authors A.G. is supported by MINECO and Generalitat Valenciana, Spain, under Grants No. FPA2011-29854-C04 and No. PROMETEOII/2014/019. A.J. acknowledges financial support from the Spanish Ministerio de Ciencia e Innovación under Contract No. FPA2011-29854-C04-01.

[1] A. Klimkiewicz *et al.*, Phys. Rev. C **76**, 051603 (2007).
[2] A. Carbone, G. Colò, A. Bracco, L.-G. Cao, P. F. Bortignon, F. Camera, and O. Wieland, Phys. Rev. C **81**, 041301(R) (2010).
[3] O. Wieland *et al.*, Phys. Rev. Lett. **102**, 9, 092502 (2009).
[4] A. Tamii *et al.*, Phys. Rev. Lett. **107**, 062502 (2011).
[5] X. Roca-Maza, G. Pozzi, M. Brenna, K. Mizuyama, and G. Colò, Phys. Rev. C **85**, 024601 (2012).
[6] X. Viñas *et al.*, Phys. J. A **50**, 27 (2014).
[7] N. Paar *et al.*, Rep. Prog. Phys. **70**, 691 (2007).
[8] D. Savran *et al.*, Prog. Part. Nucl. Phys. **70**, 210 (2013).
[9] T. D. Poelhekken *et al.*, Phys. Lett. B **278**, 423 (1992).
[10] D. Savran *et al.*, Phys. Rev. Lett. **97**, 172502 (2006).
[11] J. Endres *et al.*, Phys. Rev. Lett. **105**, 212503 (2010).
[12] J. Endres *et al.*, Phys. Rev. C **85**, 064331 (2012).
[13] V. Derya *et al.*, Phys. Lett. B **730**, 288 (2014).
[14] F. C. L. Crespi *et al.*, Phys. Rev. Lett. **113**, 012501 (2014).
[15] L. Pellegri *et al.*, Phys. Lett. B **738**, 519 (2014).
[16] M. Krzysiek *et al.*, Phys. Scr. **89**, 054016 (2014).
[17] R. Schwengner *et al.*, Phys. Rev. C **78**, 064314 (2008).
[18] C. Iwamoto *et al.*, Phys. Rev. Lett. **108**, 262501 (2012).
[19] J. R. Beene *et al.*, Phys. Rev. C **39**, 4, 1307 (1989).
[20] J. R. Beene *et al.*, Phys. Rev. C **41**, 920 (1990).
[21] R. Liguori Neto *et al.*, Nucl. Phys. A **560**, 733 (1993).
[22] D. Mengoni *et al.*, Nucl. Instrum. Methods Phys. Res., Sect. A **764**, 241 (2014).
[23] S. Akkoyun *et al.*, Nucl. Instrum. Methods Phys. Res., Sect. A **668**, 26 (2012).
[24] A. Gadea *et al.*, Nucl. Instrum. Methods Phys. Res., Sect. A **654**, 88 (2011).
[25] S. Agostinelli *et al.*, Nucl. Instrum. Methods Phys. Res., Sect. A **506**, 250 (2003).
[26] E. Farnea *et al.*, Nucl. Instrum. Methods Phys. Res., Sect. A **621**, 331 (2010).
[27] I. J. Thompson, Computer code FRESCO [http://www.fresco.org.uk/index.htm].
[28] I. J. Thompson, Comput. Phys. Rep. **7**, 167 (1988).
[29] J. Heisenberg *et al.*, Phys. Rev. C **29**, 97 (1984).
[30] E. Lanza, A. Vitturi, M. V. Andrés, F. Catara, and D. Gambacurta, Phys. Rev. C **84**, 064602 (2011).